

Synthesis of nanocrystalline δ -MoN by thermal annealing of amorphous thin films grown on (100) Si by reactive DC sputtering at room temperature

N. Haberkorn,^{1,2} S. Bengio,¹ H. Troiani,^{1,2} S. Suárez,^{1,2} P. D. Pérez,¹ M. Sirena,^{1,2} J. Guimpel.^{1,2}

¹*Consejo Nacional de Investigaciones Científicas y Técnicas, Centro Atómico Bariloche, Av. Bustillo 9500, 8400 San Carlos de Bariloche, Argentina.*

²*Instituto Balseiro, Universidad Nacional de Cuyo, Av. Bustillo 9500, 8400 San Carlos de Bariloche, Argentina*

We report on the synthesis and characterization of nanocrystalline δ -MoN by recrystallization of amorphous thin films grown on (100) Si by DC sputtering at room temperature. Films with chemical composition MoN were grown by reactive sputtering using a deposition pressure of 5mTorr with a reactive mixture of Ar/(Ar+N₂)=0.5. Initially the films display an amorphous structure with a residual-resistivity ratio ($RRR = R^{300K}/R^{\text{onset}} \approx 0.8$). After the thermal annealing at temperatures above 600 °C, the films crystallize in the hexagonal δ -MoN phase and display $RRR > 1$. After annealing at 700 °C for 30 minutes, the films display nanometric grains (≈ 10 nm) and a superconducting critical temperature $T_c = 11.2$ K (close to the one reported for bulk specimens: 13 K). The films display very smooth surfaces, a property which is relevant for technological applications, such as the design of superconductive devices, i.e. Josephson tunnel junctions. Our results provide a simple method to synthesize superconducting thin films on silicon wafers with T_c above the ones observed for conventional superconductors such as Nb.

1. Introduction

The synthesis of superconducting transition-metal nitrides is of technological relevance in the design of devices such as tunnel junctions [1] and electromagnetic radiation detectors [2,3]. The molybdenum nitrides possess several superconducting crystalline phases: γ -Mo₂N (cubic) with $T_c \sim 5$ K [4], β -Mo₂N (tetragonal) with $T_c \sim 5$ K [5] and δ -MoN (hexagonal) with $T_c \sim 13$ K [6,7]. Thin films of the different crystalline structures have been sintered through chemical and physical routes [8,9,10,11,12,13]. An outstanding feature for γ -Mo₂N and δ -MoN is that sharp superconducting transitions have been observed for epitaxial and polycrystalline thin films [14,15,16]. Moreover, superconductivity has been observed for films with thicknesses of a few nanometers [14,15,17]. Recently, we have reported that the chemical concentration and T_c for Mo-N thin films grown at room temperature by reactive DC sputtering can be modified by changing the Ar:N₂ ratio [18]. Films grown with $N_2/(Ar+N_2) < 0.4$ mixtures are superconductive with nanocrystalline γ -Mo₂N phase. Films grown with $N_2/(Ar+N_2) > 0.4$ mixtures are amorphous with a stoichiometry Mo/N ≈ 1 (close to the one corresponding to δ -MoN). These amorphous films do not display superconducting transition. It is worth noting that the δ -MoN phase displays T_c higher than Nb (hence, displays larger superconducting gap $\Delta = 1.76.k_B.T_c$). In addition, hexagonal δ -MoN is the hardest superconductor metal nitride (relevant for coating) [7].

In this work, we report the synthesis of nanocrystalline δ -MoN by recrystallization of amorphous thin films. Initially, stoichiometric MoN thin films are grown by reactive DC sputtering at room temperature on a 8 nm thick buffered (100) Si using a $N_2/(Ar+N_2) = 0.5$ mixture. As-grown thin films display a residual-resistivity ratio ($RRR = R^{300K}/R^{\text{onset}} \approx 0.8$, metallic behavior ($RRR > 1$) and superconductivity emerge after annealing the films at temperatures above 600 °C. Thin films annealed at 700 °C for 30 minutes in vacuum display smooth surfaces and superconducting critical temperature up to 11.2 K (close to the one reported for bulk). The successful synthesis of δ -MoN thin films on Si substrates by a

controllable and reproducible route (with low roughness values), enhances the potential applications in superconducting devices.

2. Material and methods

MoN films were deposited on 8 nm thick AlN buffered Si(100) substrates by reactive DC magnetron sputtering using a $N_2/(Ar+N_2) = 0.5$ mixture without any intentional heating of the substrate [17,18]. The AlN buffer layer was introduced to avoid any chemical reaction between the Mo and the SiO_2 cap layer of the Si wafers. The residual pressure of the chamber was less than 10^{-6} Torr. Ultra-high purity Ar (99.999%) and N_2 (99.999%) were used as gas sources. The AlN and MoN layers were grown by RF (100 W) and DC (50 W) magnetron sputtering, respectively. During deposition the target to substrate distance was ~ 5.5 cm. The total pressure at the chamber was 5mTorr. Al:N buffer layers were grown using a $N_2/(Ar+N_2) = 0.2$ mixture. The deposition rate for MoN using a $N_2/(Ar+N_2) = 0.5$ mixture was ≈ 17 nm / min. Thermal annealing was performed in vacuum (to avoid surface contamination) with a residual pressure of 10^{-5} Torr at temperatures between 400 °C and 700 °C during periods of 30 min. In order to homogenize the temperature, the films were enveloped in a tantalum foil during the annealing procedure. Wherever used, the notation [X] corresponds to samples annealed at X °C (with X = 400 °C, 600 °C and 700°C) for 30 min. The results shown here correspond to 170 nm thick MoN films (deposition time of 10 minutes).

X-diffraction patterns were obtained with a Panalitcal Empirean equipment. The structure of [700] was studied by transmission electron microscopy (TEM) with a Philips CM200UT microscope operating at 200 kV. The TEM specimen was prepared by scraping the surface of a film with a diamond tip. The topology of the films was characterized by atomic force microscopy (AFM) measurements in a Dimension 3100©Brucker microscope. The AFM images were obtained in tapping mode. The chemical composition and thickness of the films were analyzed by Rutherford Backscattering Spectroscopy (RBS) with a TANDEM

accelerator using a 2 MeV 4He^{2+} ion beam. Surface composition analysis was performed by X-ray photoelectron spectroscopy (XPS) using a standard Al/Mg twin-anode X-ray gun and a hemispherical electrostatic electron energy analyzer (high vacuum conditions with a base pressure of 10^{-9} Torr). The electrical transport measurements were performed using the standard four-point configuration.

3. Results and discussion

The chemical composition of the films was verified using RBS. The composition $\text{MoN}_{(1.00 \pm 0.05)}$ was observed for pristine and annealed specimens. As-grown MoN thin films using a $\text{N}_2/(\text{Ar}+\text{N}_2)=0.5$ mixture are amorphous [18]. The crystallization of δ -MoN after thermal annealing at temperatures above 600 °C was confirmed by X-ray diffraction (XRD) analysis. Figure 1 shows the XRD diffraction pattern for [600] where the peaks (002), (200) and (202) corresponding to the hexagonal δ -MoN phase are observed. No significant changes were noted in the X-ray diffraction for [700], compared to [600]. The lattice parameters of δ -MoN film, calculated from the (002) and (200) diffraction peaks, are $a = 0.572(2)$ nm and $c = 0.555(3)$ nm. These values are close to those observed in epitaxial δ -MoN [12]. Figures 2*ab* show TEM images for [700]. Fig. 2*a* shows a cross section bright field TEM image where the film thickness homogeneity can be observed. Figure 2*b* shows a dark field image obtained from the $(200)_{\delta\text{-MoN}}$ ring (see selected area electron diffraction (SAED) in the inset). The bright regions in the image correspond to nanometric δ -MoN grains with typical size between 5 nm and 10 nm. In addition, the 201 reflection - corresponding to a superficial MoO_3 layer- is observed in the SAED [17]. Figure 3*a* shows the AFM image for [700]. The film displays a very smooth surface, only a few small morphologic inhomogeneities with a height less than 6 nm are observed (see profile in Fig. 3*b*). The Root Mean Square (RMS) roughness for an area of $5 \mu\text{m}^2$ is 0.6 nm, which indicates that (compared to as-grown films) recrystallization does not significantly alter the morphology of the films [17]. The weak influence of the annealing and recrystallization in the surface topology can be attributed to the crystallization of grains of a few nanometers.

XPS measurements were performed to obtain information about the chemical composition of the film and the chemical state of the Mo. The photoelectron peaks Mo3d, O1s, C1s and N1s were measured in detail. An overlap of the N1s and the Mo3p peaks was observed. In order to remove components related to superficial C and MoO₃, the surface of the films was cleaned with Ar⁺ sputtering (2kV) [17]. The Mo3d binding energy region for the surface of as-grown films and [700] thin films is shown in Figs. 4a and 4b, respectively. In the as-grown Mo3d spectra two components were identified: a major component at BE= 228.9eV attributed to the δ -MoN phase, and a minor component at BE=228.5eV attributed to the γ -Mo₂N phase [19,20]. In the [700-A] thin films only one major component was identified at BE=228.9eV assigned to the δ -MoN phase. Besides, in both spectra there is an extra component at higher binding energies that can be ascribed to different causes: unscreened peaks of the present phases as observed for MoO₂ [21], the presence of Mo⁴⁺ associated to MoO₂ impurities or as a consequence of overlooking possible asymmetric behavior of the main components, as suggested for MoO₂ [22].

Then, the electrical properties were analyzed by measuring the electrical resistance as function of the temperature and the applied magnetic field. Figure 5a presents the temperature dependent electrical resistance under a zero applied magnetic field. As-grown thin films display a $RRR \approx 0.81$ (indicative of high disorder with very short electronic mean free path l). After crystallization to δ -MoN (at ≈ 600 °C), the films show a metallic behavior. For [600] and [700], the RRR values are ≈ 1.3 and ≈ 1.5 , and they display a superconducting transition with $T_c = 10.5$ K and 11.2 K, respectively (see inset Fig. 5a).

The superconducting transition width (defined as the temperature window corresponding to a resistance change from 90% to 10% of the normal resistance) is ≈ 1 K for both samples. For longer annealing periods (> 30 min) or for higher annealing temperatures (> 700 °C), neither T_c is increased nor the superconducting transition width, reduced. In particular, annealing temperatures higher than 800 °C produce cracks on the surface, which is evidenced in wider superconducting transitions without percolation. Finally, we analyzed the temperature dependence of the upper critical field $H_{c2}(T)$. Figure 5b shows $H_{c2}(T)$ for the [600] and [700] with the magnetic field perpendicular (H_{c2}^{\perp}) and parallel (H_{c2}^{\parallel}) to the surface. Inset in Fig. 5b shows the typical resistance vs. temperature curves for different

applied magnetic fields ($\mu_0 H = 0, 2 \text{ T}, 4 \text{ T}$ and 6 T). The results show negligible upper critical field anisotropy ($\gamma = H_{c2}^\perp / H_{c2}'' \approx 1$), which is in agreement with the expectations for polycrystalline thin films for the 3 dimensional limit (thickness $\gg \xi(0)$). The temperature dependence of H_{c2}^\perp can be analyzed by the WHH model developed for dirty one-band superconductors [23], which is given by:

$$\ln \frac{1}{t} = \sum_{v=-\infty}^{\infty} \left(\frac{1}{|2v+1|} - \left[|2v+1| + \frac{\hbar}{t} + \frac{(\alpha \hbar/t)^2}{|2v+1| + (\hbar + \lambda_{so})/t} \right]^{-1} \right) \text{ [eq. 1]},$$

where $t = T / T_c$, $\hbar = (4/\pi^2)(H_{c2}(T)/|dH_{c2}/dT|_{T_c})$, α is the Maki parameter (quantifies the weakening influence of the Pauli electron spin paramagnetism on the superconducting state), and λ_{so} is the spin-orbit scattering constant. When $\lambda_{so} = 0$, $H_{c2}(0)$ -obtained from the WHH formula- satisfies the relation $H_{c2}(0) = \frac{H_{c2}^{orb}(0)}{\sqrt{1+\alpha^2}}$ [eq. 2], which is originally derived by K. Maki [24]. Considering $\alpha = 0$ and $\lambda_{so} = 0$ in the WHH model, the $H_{c2}(T)$ curves obtained in the analyzed samples were as expected. To adjust the data, $-|dH_{c2}/dT|_{T_c} \approx 1 \text{ T/K}$ was used. For $\alpha = 0$, $H_{c2}(T)$ was given as the pure “orbital field limit” ($H_{orb}(T)$), due to the supercurrents circulating around the vortex cores. The $H_{c2}(0)$ obtained from the extrapolation to zero field of the WHH model are 7.5 T ($\xi(0) = 6.6 \text{ nm}$) and 7.8 T ($\xi(0) = 6.5 \text{ nm}$) for [600] and [700], respectively. These values are lower than the $\approx 10 \text{ T}$ previously obtained in epitaxial and dirty δ -MoN sintered for polymer assisted deposition [25]. For weakly coupled BCS superconductor $\xi_0 = 0.18 \frac{\eta v_F}{k_B T_c}$ (where v_F is the Fermi velocity) [26]. Similar $\xi_0 T_c$ values ($\approx 70 \text{ nm} \cdot \text{K}$) are obtained for [600] and [700] and the films reported in Ref [25] ($\xi_0 T_c = 5.6 \text{ nm} \cdot 12.6 \text{ K}$), which indicates that the reduction in $H_{c2}(0)$ can be mainly attributed to the suppression in T_c (corresponding to films in the dirty limit with very short electronic mean free path l).

4. Conclusions

In summary, we report on the synthesis and the resulting superconducting properties in nanocrystalline δ -MoN thin films. Initially, amorphous MoN thin films were grown by DC sputtering at room temperature on Si wafers. In a second step, the films were recrystallized in vacuum (to avoid surface contamination) at temperatures between 600 °C and 700 °C. The annealed films display very smooth surfaces (relevant for tunnel junctions) and a polycrystalline microstructure with nanometric grains (typical size 5-10 nm). The superconducting critical temperature T_c for films annealed at 700 °C is 11.2 K (close to the 13 K reported for bulk). The reported simple process to synthesize δ -MoN thin films with adequate physical properties on Si substrates enhances its potential for developing different technological applications, varying from radiation sensors to Josephson tunnel junctions.

Acknowledgments

We thank C. Olivares for technical assistance. This work was partially supported by the ANPCYT (PICT 2015-2171), U. N. de Cuyo 06/C505 and CONICET PIP 2015-0100575CO. NH, SB, MS and JG are members of the Instituto de Nanociencia y Nanotecnología, CNEA-CONICET.

Figure 1. X-ray diffraction pattern for a 170 nm MoN thin film after being annealed at 600 °C for 30 min. (*) Reflections from the sample holder.

Figure 2. TEM images for a 170 nm thick δ -MoN film ([700]). *a*) Bright field cross section TEM image. *b*) Dark field plan view image using the (002) $_{\delta}$ -MoN. Inset shows the corresponding SAED pattern.

Figure 3. *a*) 5 x 5 μm^2 topographical AFM of a 170 nm thick MoN film after being annealed at 700 °C. *b*) AFM profile for the line indicated in *a*).

Figure 4. XPS Mo3d spectra of: *a*) As-grown MoN thin films. *b*) MoN film after being annealed at 700 °C ([700]).

Figure 5. *a)* Temperature dependence of the resistance for an as-grown thin film, [400], [600] and [700]. Inset shows the temperature dependence of [600] and [700] at temperatures smaller than 20 K and the criteria for the determination of T_c . *b)* Temperature dependence of the upper critical field (H_{c2}) with \mathbf{H} parallel and perpendicular to the surface for [600] and [700]. Inset shows the temperature dependence of the resistance for [600] and [700] applying different magnetic field \mathbf{H} perpendicular to the surface.

Figure 1

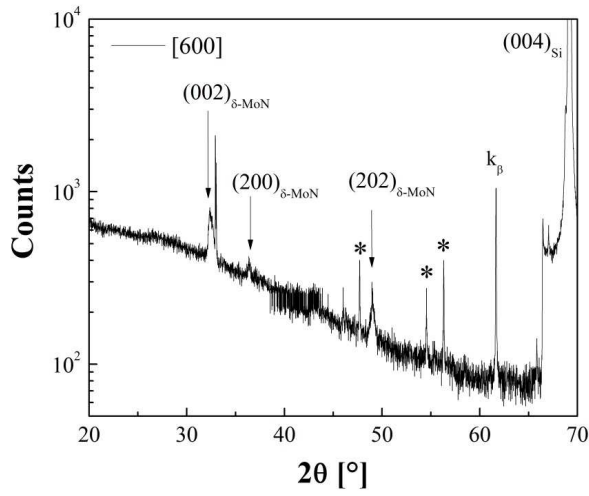


Figure 2

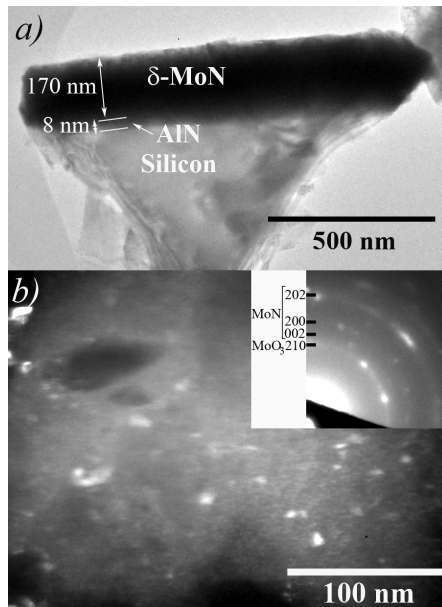


Figure 3

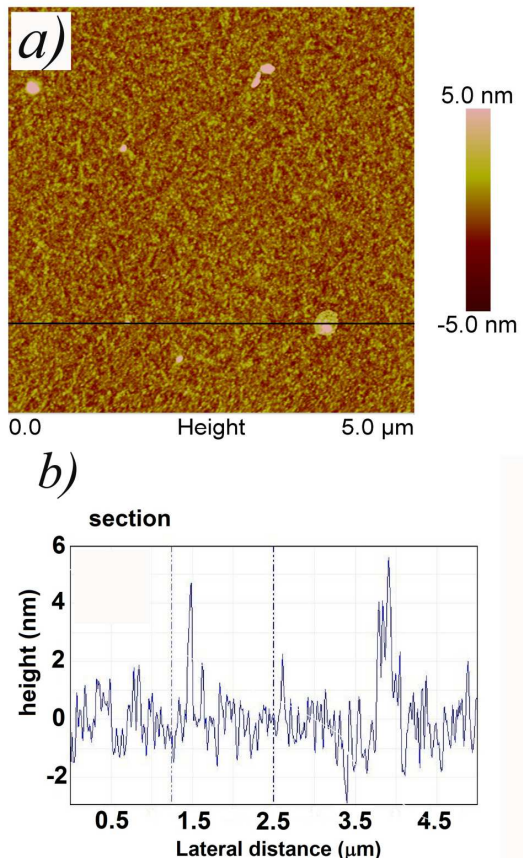


Figure 4

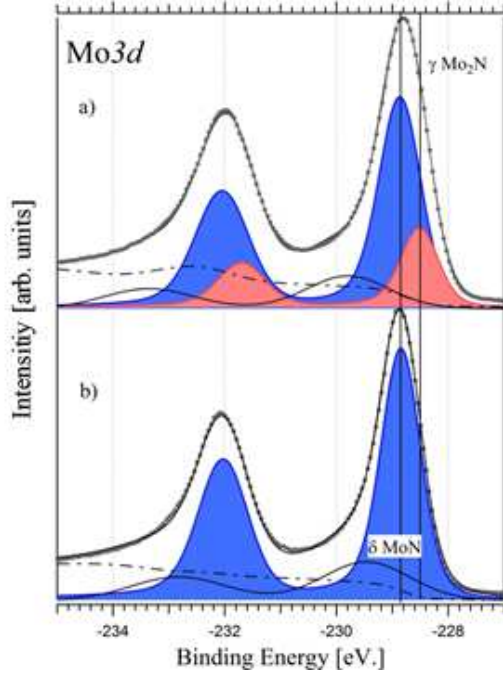
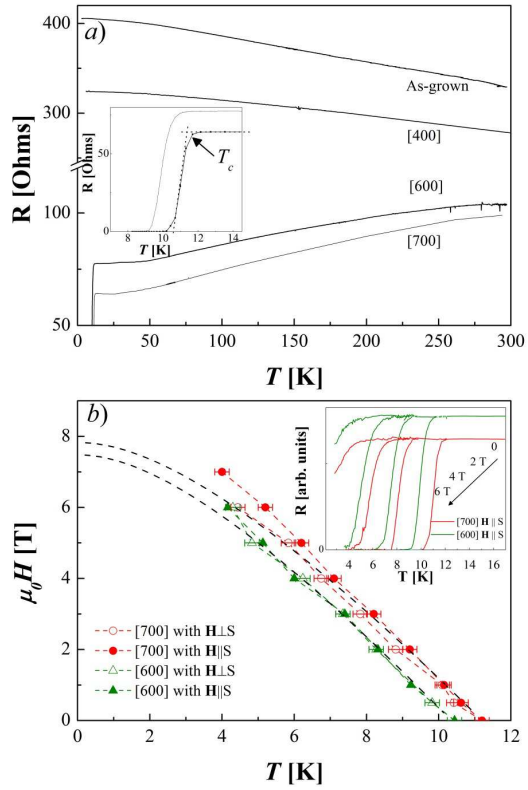


Figure 5



-
- [1] Zhen Wang, Hirotaka Terai, Akira Kawakami, Yoshinori Uzawa, Interface and tunneling barrier heights of NbN/AlN/NbN tunnel junctions, *Appl. Phys. Lett.*, **75** (1999) 701-703.
- [2] M. Shcherbatenko, I. Tretyakov, Yu. Lobanov, S. N. Maslennikov, N. Kaurova, M. Finkel, B. Voronov, G. Goltsman, T. M. Klapwijk, Nonequilibrium interpretation of DC properties of NbN superconducting hot electron bolometers, *Appl. Phys. Lett.* **109** (2016) 132602-132605.
- [3] Chandra M. Natarajan, Michael G. Tanner, Robert H. Hadfield, Superconducting nanowire single-photon detectors: physics and applications, *Supercond. Sci. Technol.* **25** (2012) 063001 (16pp).
- [4] B. T. Matthias, J. K. Hulm, A Search for New Superconducting Compounds, *Phys. Rev.* **87** (1952) 799-806.
- [5] Kei Inumaru, Kazuya Baba, Shoji Yamanaka, Synthesis and Characterization of Superconducting β -Mo₂N Crystalline Phase on a Si Substrate: An Application of Pulsed Laser Deposition to Nitride Chemistry, *Chem. Mater.* **17** (2005) 5935-5940.
- [6] Kei Inumaru, Takanori Nishikawa, Kazuharu Nakamura, Shoji Yamanaka, High-Pressure Synthesis of Superconducting Molybdenum Nitride δ -MoN by in Situ Nitridation, *Chem. Mater.* **20** (2008) 4756-4761.
- [7] Shanmin Wang, Daniel Antonio, Xiaohui Yu, Jianzhong Zhang, Andrew L. Cornelius, Duanwei He, Yusheng Zhao, The Hardest Superconducting Metal Nitride, *Scient. Rep.* **5** (2015) 13733 (8 pp).
- [8] Y. H. Shi, B. R. Zhao, Y. Y. Zhao, L. Li, J. R. Liu, Superconducting and normal-state properties of MoN_x thin films, *Phys. Rev B* **38** (1988) 4488-4491.
- [9] H. Ihara, M. Hirabayashi, K. Senzaki, Y. Kimura, H. Kezuka, Superconductivity of B1-MoN films annealed under high pressure, *Phys. Rev. B* **32** (1985) 1816-1817.
- [10] Kei Inumaru, Kazuya Baba, Shoji Yamanaka, Structural distortion and suppression of superconductivity in stoichiometric B1-MoN epitaxial thin films, *Phys. Rev. B* **73** (2006) 52504 (4pp).
- [11] D. K. Christen, S. T. Sekula, J. T. Ellis, J. D. Lewis, J. M. Williams, Formation, properties, and ion irradiation effects of hexagonal structure MoN thin films., *IEEE Trans. Magn.*, **23** (1987), 1014-1018.
- [12] Y. Y. Zhang *et al.*, Epitaxial Superconducting δ -MoN Films Grown by a Chemical Solution Method, *J. Am. Chem. Soc.* **133**(2011) 20735-20737.
- [13] Hongmei Luo, Guifu Zou, Haiyan Wang, Joon Hwan Lee, Yuan Lin, Huisheng Peng, Qianglu Lin, Shuguang Deng, Eve Bauer, T. Mark McCleskey, Anthony K. Burrell, Quanxi Jia, Controlling Crystal Structure and Oxidation State in Molybdenum Nitrides through Epitaxial Stabilization. *J. Phys. Chem. C* **115** (2011) 17880-17883.
- [14] Takuya Tsuneoka, Kazumasa Makise, Sho Maeda, Bunju Shinozaki, Fusao Ichikawa, Localization and pair breaking parameter in superconducting molybdenum nitride thin films, *J. Phys.: Condens. Matter* **29** (2017) 015701 (7 pp).
- [15] Hanlu Zhang *et al.*, Self-assembled *c*-axis oriented δ -MoN thin films on Si substrates by chemical solution deposition: Growth, transport and superconducting J. *Alloys Compounds* **704** (2017) 453-458.
- [16] R. Baskaran, A. V. Thanikai Arasu, E. P. Amaladass, L. S. Vaidhyanathan, D. K. Baisnab, Increased upper critical field for nanocrystalline MoN thin films deposited on AlN buffered substrates at ambient temperature, *J. Phys. D* **49** (2016) 205304-205307.
- [17] N. Haberkorn, S. Bengio, H. Troiani, S. Suárez, P. D. Pérez, P. Granell, F. Golmar, M. Sirena, J. Guimpel, Thickness dependence of the superconducting properties of γ -Mo₂N thin films on Si (001) grown by DC sputtering at room temperature, *Materials Chem. Phys.* **204** (2018) 48-57.
- [18] N. Haberkorn, S. Bengio, S. Suárez, P. D. Pérez, M. Sirena, J. Guimpel, Effect of the nitrogen-argon gas mixtures on the superconductivity properties of reactively sputtered molybdenum nitride thin films, *Mat. Lett.* **215**(2018) 15-18.
- [19] Kejun Zhang, Lixue Zhang, Xiao Chen, Xiang He, Xiaogang Wang, Shanmu Dong, Lin Gu, Zhihong Liu, Changshui Huang, Guanglei Cui, Molybdenum Nitride/N-Doped Carbon Nanospheres for Lithium-O₂ Battery Cathode Electrocatalyst, *Appl. Mat. Interfaces* **5** (2013) 3677-3682.
- [20] Z. B. Zhaobin Wei, P. Grange, B. Delmon, XPS and XRD studies of fresh and sulfided Mo₂N, *Appl. Surf. Sci.* **135** (1998) 107-114.
- [21] David O. Scanlon, Graeme W. Watson, D. J. Payne, G. R. Atkinson, R. G. Egdell and D. S. L. Law, Theoretical and Experimental Study of the Electronic Structures of MoO₃ and MoO₂, *J. Phys. Chem. C* **114** (2010) 4636-4645.

-
- [22] J. Baltrusaitis, B. Mendoza-Sanchez, V. Fernandez, R. Veenstra, N. Dukstiene, A. Robert, N. Fairley, Generalized molybdenum oxide surface chemical state XPS determination via informed amorphous sample model, *Appl. Surf. Scie* **326** (2015) 151-161.
- [23] N. R. Werthamer, E. Helfand, P. C. Hohenberg, Temperature and Purity Dependence of the Superconducting Critical Field, Hc2. III. Electron Spin and Spin-Orbit Effects, *Phys. Rev.* **147** (1966) 295-302.
- [24] K. Maki, Effect of Pauli Paramagnetism on Magnetic Properties of High-Field Superconductors, *Phys. Rev.* **148** (1966) 362-369.
- [25] N. Haberkorn, Y.Y. Zhang, J. Kim, T.M. McCleskey, A.K. Burrell, R.F. Depaula, T. Tajima, Q.X. Jia, L. Civale, Upper critical magnetic field and vortex-free state in very thin epitaxial d-MoN films grown by polymer-assisted deposition, *Supercond. Sci. Technol.* **26** (2013) 105023 (7 pp).
- [26] M. Tinkham, *Introduction to superconductivity*, 2 edition ed. (Dover Publications, New York, 2004).